

The cluster relic source in A 521

S. Giacintucci^{a,b,c} T. Venturi^b S. Bardelli^a G. Brunetti^b
R. Cassano^c D. Dallacasa^{b,c}

^a*INAF – Osservatorio Astronomico di Bologna, via Ranzani 1, I-40126 Bologna, Italy*

^b*INAF – Istituto di Radioastronomia, via Gobetti 101, I-40129, Bologna, Italy*

^c*Dipartimento di Astronomia, Università di Bologna, via Ranzani 1, I-40126, Bologna, Italy*

Abstract

We present high sensitivity radio observations of the merging cluster A 521, at a mean redshift $z=0.247$. The observations were carried out with the GMRT at 610 MHz and cover a region of ~ 1 square degree, with a sensitivity limit of $1\sigma = 35 \mu\text{Jy b}^{-1}$.

The most relevant result of these observations is the presence of a radio relic at the cluster periphery, at the edge of a region where group infalling into the main cluster is taking place. Thanks to the wealth of information available in the literature in the optical and X-ray bands, a multi-band study of the relic and its surroundings was performed. Our analysis is suggestive of a connection between this source and the complex ongoing merger in the A 521 region. The relic might be “revived” fossil radio plasma through adiabatic compression of the magnetic field or shock re-acceleration due to the merger events. We also briefly discussed the possibility that this source is the result of induced ram pressure stripping of radio lobes associated with the nearby cluster radio galaxy J0454–1016a.

Allowing for the large uncertainties due to the small statistics, the number of radio emitting early-type galaxies found in A 521 is consistent with the expectations from the standard radio luminosity function for local ($z \leq 0.09$) cluster ellipticals.

Key words: radio continuum : galaxies, galaxies: clusters: general, galaxies: clusters: individual: A 521

PACS: 98.65.Cw, 98.65.Hb, 95.85.Bh

1 Introduction

Radio observations reveal that a number of galaxy clusters host diffuse synchrotron radio emission, not obviously associated with cluster galaxies, ex-

tended on cluster scale and referred to as *radio halos* and *relics*. These sources probe the presence of magnetic fields and relativistic particles mixed with the hot gas in the intracluster medium (ICM). A promising approach in our understanding of the nature of these sources is the possibility that turbulence and shocks induced by cluster mergers may be able to re-accelerate pre-existing electrons in the ICM, producing the emission from radio halos and relics (see the recent reviews by Brunetti 2003 and 2004, Sarazin 2004).

Both halos and relics are characterised by very low surface brightness. They lack an obvious optical counterpart and can reach sizes \gtrsim Mpc. The class of radio halos is at present well defined (see Giovannini & Feretti 2002 for a review). Halos are detected in the central regions of galaxy clusters, show a fairly regular shape, and are usually unpolarized. They are characterised by steep integrated radio spectra, i.e. $\alpha \gtrsim 1$ for $S \propto \nu^{-\alpha}$, although the spectral index distribution may show small scale inhomogeneities (Feretti et al. 2004). High frequency spectral steepening is present in few cases (Feretti 2005, Giacintucci et al. 2005).

Cluster relic sources are less homogeneous and more difficult to classify, possibly due to our still limited knowledge and understanding of their formation and evolution. They are usually located in peripheral cluster regions, and show many different morphologies (sheet, arc, irregular, toroidal). At present ~ 20 relics and candidates are known (Kempner & Sarazin 2001; Giovannini & Feretti 2004), however the observational information is still limited. Their radio emission is usually highly polarized (up to 30%). For those few sources with multifrequency imaging, a steep integrated spectrum is found ($\alpha \gtrsim 1$, up to ultra-steep regimes).

All clusters known to host a radio halo and/or a relic source are found to show some degree of disturbance in the distribution of the hot gas and of the optical galaxies (Buote 2001, Schuecker et al. 2001, Sarazin 2002). Some well studied and impressive examples are for instance the radio halo in A 2163 (Feretti et al. 2001) and the double relics in A 3667 (Roettiger et al. 1999) and A 3367 (Bagchi et al. 2005).

It is interesting to point out that the observational link between cluster halos, relics and the merging phenomena has been outlined *a posteriori*. A different and promising approach is the *a priori* selection of clusters experiencing well studied merging events, in order to determine the occurrence of halos and relics. As an example, deep radio observations of the merging chain of clusters in the core of the Shapley Concentration led to the discovery of a radio halo at the centre of A 3562, which is the faintest radio halo known to date (Venturi et al. 2000 and 2003, Giacintucci et al. 2004 and 2005), and given its very low surface brightness it would have not been detected in a “blind” radio survey.

In this paper we present Giant Metrewave Radio Telescope (GMRT) 610 MHz

observations of the galaxy cluster A 521. This cluster was selected for the search of extended cluster scale radio emission on the basis of the wealth of optical (Maurogordato et al. 2000, hereinafter M00; Ferrari et al. 2003, hereinafter F03) and X-ray (Arnaud et al. 2000, hereinafter A00; Ferrari et al. 2005, hereinafter F05) information available in the literature, suggesting a very complex dynamical state. Furthermore, thanks to the amount of photometric and spectroscopic data available, A 521 is also an ideal environment to study the effects of cluster mergers on the radio emission properties of the member galaxy population, which is still controversial (see e.g. Venturi et al. 2000, Giacintucci et al. 2004, Owen et al. 1999, Miller & Owen 2003, Miller et al. 2003).

The observations presented here are part of a much larger project carried out with a deep GMRT radio survey at 610 MHz (Venturi et al. in prep.), whose aim is the search for radio halos and relics in clusters at intermediate redshift ($z=0.2\div 0.4$), to test current statistical expectations from models for the formation of cluster radio halos (Cassano et al. 2004; Cassano & Brunetti 2005; Cassano et al. in prep.).

The outline of the paper is as follows: in Section 2 we give a summary of the main properties of A 521 and its complex dynamical state of merging; the 610 MHz observations and the data reduction are described in Section 3; in Section 4 we present the radio source sample in the A 521 region; in Section 5 we give the radio–optical identifications and present the nuclear radio activity of cluster early–type galaxies; the relic radio source is presented in Section 6; the discussion is carried out in Section 7; our conclusions are summarized in Section 8.

Throughout the paper we assume $H_0 = 70 \text{ km s}^{-1} \text{ Mpc}^{-1}$, $\Omega_m=0.3$ and $\Omega_\Lambda=0.7$. At the average redshift of A 521 ($z = 0.247$), this cosmology leads to a linear scale of $1 \text{ arcsec} = 3.87 \text{ kpc}$.

2 The cluster Abell 521

Abell 521 is a rich galaxy cluster, located at a mean redshift $z=0.247$. Its general properties are given in Table 1. Note that the cluster coordinates in the table are those of the ROSAT/HRI X-ray centre (A00); the X-ray luminosity (0.1–2 keV band) is from Böhringer et al. 2004 (REFLEX galaxy cluster catalogue); the velocity dispersion σ_v is from F03; the temperature value is taken from A00; the virial mass M_V was computed from the L_X – M_V relation in Reiprich & Böhringer (2002), adopting the cosmology used in this paper; R_V is the corresponding virial radius.

Table 1
Properties of the cluster A 521.

RA_{J2000}	$04^h 54^m 08.6^s$
DEC_{J2000}	$-10^\circ 14' 39.0''$
Bautz–Morgan Class	III
Richness	1
Redshift	0.247
σ_v (km s ⁻¹)	1325
L_X (10 ⁴⁴ erg s ⁻¹)	8.178
T_X (keV)	6.4
M_V (M _⊙)	1.8×10^{15}
R_V (Mpc)	2.8

Detailed X–ray (A00, F05) and optical studies of A 521 (M00, F03) revealed that the dynamical state of this cluster is very complex, since it is still undergoing multiple merging events. Figure 1 sketches the scenario proposed by these authors.

From the X–ray analysis A00 concluded that the main merger episode is occurring along the North–West/South–East direction (arrow in Fig. 1), between the main cluster (G11) and a northwestern compact group (G111), whose X–ray emissions are centered on $RA=04^h 54^m 08.6^s$, $DEC=-10^\circ 14' 39.0''$ and $RA=04^h 54^m 05.8^s$, $DEC=-10^\circ 13' 00.4''$ respectively. The gas mass ratio between G11 and G111 components is $M_{\text{gas,main}}/M_{\text{gas,sub}} \sim 7$ (A00). In their more recent analysis F05 reported a misalignment between the X–ray and optical merger axis.

The study of the galaxy distribution and the substructure analysis carried out by F03 revealed the existence of many optical subclumps aligned along the merger direction. In particular these authors identified the following velocity groups along this axis (see Figure 1):

- G11: the main cluster with a mean velocity $\langle v \rangle = 73965$ km s⁻¹ and a velocity dispersion $\sigma \sim 930$ km s⁻¹;
- G111: a group dynamically bound to the brightest cluster galaxy (BCG), with a very low velocity dispersion ($\sigma \sim 250$ km s⁻¹) and a slightly higher mean velocity ($\langle v \rangle = 74290$ km s⁻¹) as compared to the main cluster G11. This group is associated with the compact X–ray group detected by A00, which is probably falling onto the cluster from the NW direction. The small difference in the mean velocity between G111 and G11 suggests that the merging is likely

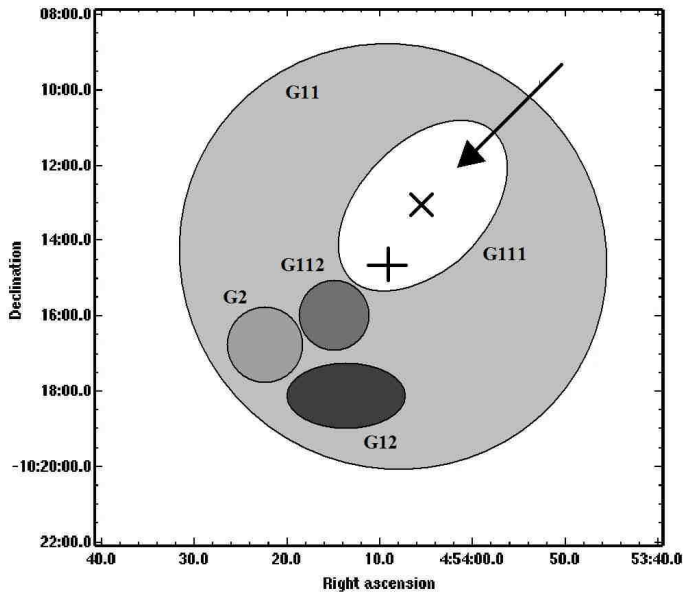


Fig. 1. Cartoon representing the substructures in A 521. The cross marks the X-ray centre of the main cluster G11, and the x-point indicates the centre of the X-ray compact group associated with the optical group G111 (see A00). The arrow represents the possible infalling direction of G111.

to take place on the plane of the sky.

– G112: a compact group bound to the cluster, whose velocity ($\langle v \rangle = 74068 \text{ km s}^{-1}$, $\sigma \sim 570 \text{ km s}^{-1}$) is similar to that of the infalling group G111. The virial masses estimated for G111 and G112 in F03 on the basis of the optical information are much smaller (\sim one order of magnitude) than that of the main cluster G11. We note that the mass ratios between G11 and the infalling groups estimated from the optical information are even larger than those derived from the X-ray data.

– G12: the lowest mass group bound to A 521, with higher velocity galaxies ($\langle v \rangle = 75730 \text{ km s}^{-1}$, $\sigma \sim 120 \text{ km s}^{-1}$).

– G2: a group South-East of A 521, at a projected distance of $\sim 900 \text{ kpc}$ from the X-ray centre of the main cluster G11. This group has a mean velocity of $\langle v \rangle = 78418 \text{ km s}^{-1}$ ($\sigma \sim 500 \text{ km s}^{-1}$), which is much higher than the cluster velocity. On the basis of the two-body criteria, F03 concluded that this group is probably not bound to A 521.

Furthermore, F03 found also evidence of a filamentary structure of galaxies in the central region of the cluster, extending along the NE-SW direction, with velocity $\langle v \rangle = 73625 \text{ km s}^{-1}$ and high velocity dispersion. This structure has been interpreted by F03 as evidence of an older merger, which occurred along a direction orthogonal to the axis of the presently ongoing merger.

Table 2
 Details of the GMRT observations for A 521.

Observation date	7 – 8 January 2005
ν	610 MHz
$\Delta\nu$	32 MHz
RA _{J2000}	04 ^h 54 ^m 09 ^s
DEC _{J2000}	−10° 14′ 19″
Primary beam	43′
Restoring beam, PA (full array)	8.6″ × 4.0″, 57°
Total Obs.time	3.5 h
rms	35 μ Jy b ^{−1}

3 Radio observations

We observed the cluster A 521 at 610 MHz with the GMRT on 7 and 8 January 2005, using simultaneously the R (USB) and L (LSB) bands of 16 MHz each, for a total frequency band of 32 MHz. Table 2 gives the details of the observations.

The observations were carried out in spectral line mode, with 128 channels in each band, with a spectral resolution of 125 kHz.

The four data sets (7 and 8 Jan 2005, USB and LSB) were analysed individually. The data calibration and reduction were performed using the NRAO Astronomical Image Processing System (AIPS) package. The sources 3C 147 and 3C 48 were observed as primary calibrators at the beginning and at the end of the observations, to determine and correct for the bandpass shape and for the initial amplitude and phase calibration. The source 0447–220 was used as secondary phase calibrator and was observed every 20 minutes throughout the observation. In order to reduce the size of the data set, after the bandpass calibration the central channels of each data set were averaged to 6 channels of ~ 2 MHz each.

For each data set, images were produced using the wide-field imaging technique, with 25 facets covering a total field of view of $\sim 1 \times 1$ square degree. After a number of phase self-calibration cycles, a final step was made, allowing for phase and amplitude corrections in order to improve the quality of the final images. The residual errors in the estimated flux density are $\lesssim 5\%$.

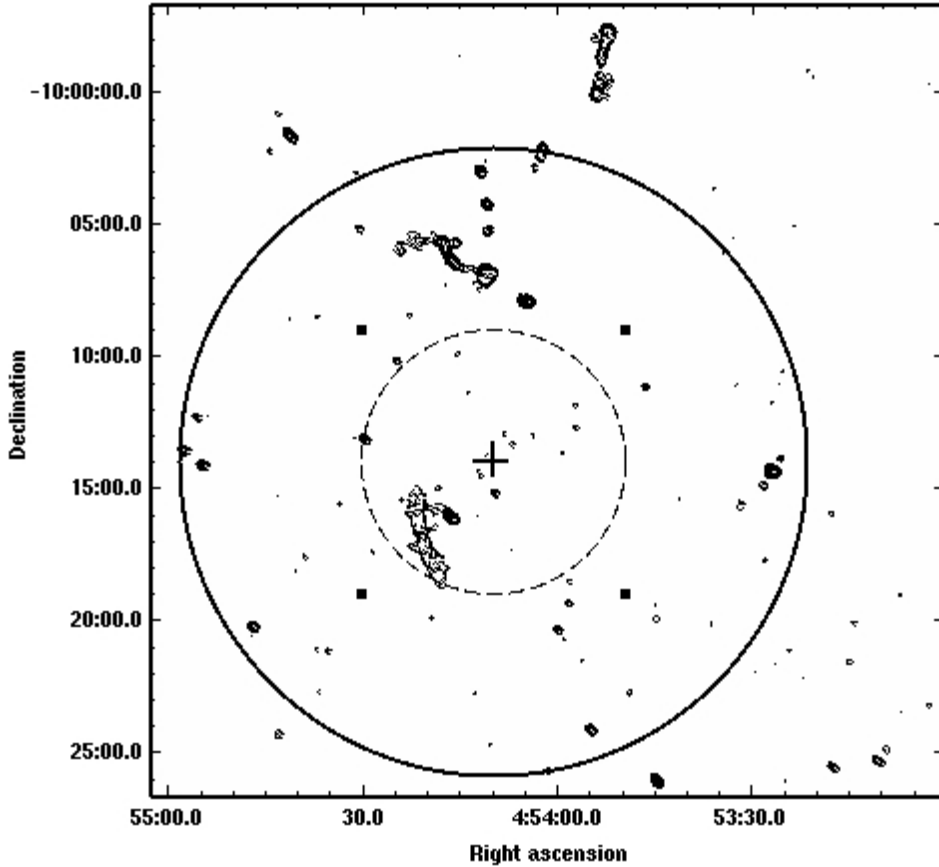


Fig. 2. 610 MHz radio contours of the $30' \times 30'$ region containing A 521. The contours are logarithmic, and the lowest level is the $5\sigma = 0.2 \text{ mJy b}^{-1}$. The resolution is $13.1'' \times 8.1''$, in p.a. 56° . The cross marks the X-ray centre of the cluster. The solid circle has a radius corresponding to the virial radius of A 521. The dashed circle indicates the region with the redshift information, and corresponds to the region shown in Fig. 3.

The four self-calibrated data sets were then averaged from 6 channels to 1 single channel and finally combined together using the AIPS task DBCON. We note that bandwidth smearing is relevant only at the edge of the wide field, and does not affect the region presented and analysed here, i.e. the inner $30' \times 30'$ (see Section 4). The images from the combined data set were obtained using again the wide-field imaging technique, combined with the task FLATN and finally corrected for the primary beam appropriate to the GMRT antennas at 610 MHz.

We produced images over a range of resolutions, reaching rms noise levels of the order of $1\sigma \sim 35 - 40 \mu\text{Jy b}^{-1}$. For the purpose of the present paper we show only the image tapered to a resolution of $13.1'' \times 8.1''$, in p.a. 56° . The 5σ detection limit in this image, 0.20 mJy b^{-1} , corresponds to a radio power limit of $3.5 \times 10^{22} \text{ W Hz}^{-1}$.

4 The sample of radio sources

The total field of view of our observations is $\sim 1^\circ \times 1^\circ$, which is much larger than the cluster size. Here we present only a portion of the whole field, with size of $30' \times 30'$, centered on RA= $04^h 53^m 00^s \div 04^h 55^m 00^s$ and DEC= $-09^\circ 55' 00'' \div -10^\circ 25' 00''$. At the cluster distance this corresponds to a region as large as $\sim 7 \times 7$ Mpc².

The 610 MHz radio emission from this region is shown in Figure 2. In the figure we also plotted a solid circle with a radius corresponding to the virial radius of A 521 (Tab. 1), and a dashed circle, representing the 5' radius region covered by the redshift catalogues in M00 and F03. The cross marks the X-ray centre of the cluster (Tab. 1).

The radio emission from the A 521 region is dominated by point-like and marginally resolved sources. However, the whole field is characterised by the presence of three extended radio sources. Two of them (see Section 5.2) are located in the northern part of the field and are associated with early-type galaxies without redshift information. The elongated structure located South-East with respect to the cluster centre is the relic source discussed in Section 6.

We used the AIPS task SAD to identify sources in the final $13.1'' \times 8.1''$ image of A 521 ($1\sigma = 40 \mu\text{Jy b}^{-1}$). Given a radio image, this task (1) finds all potential sources whose peak is brighter than a given level; (2) Gaussian components are fitted; (3) positions and flux density values are given. The task also produces a residual image, which can be inspected to identify both extended sources not well fitted by Gaussians, and sources with peak flux density lower than the previous threshold. As first step, we used SAD to find all sources with peak flux density greater than 0.32 mJy b^{-1} , i.e. 8 times the rms noise level in the field. Then, on the residual image we searched for all sources with peak flux densities in the range $5\sigma - 8\sigma$ (i.e. $0.20 - 0.32 \text{ mJy b}^{-1}$). On this image we identified also the extended sources.

Each radio source of the list was then carefully inspected, and the flux density values given by SAD for the unresolved or marginally resolved sources were checked using the task JMFIT. For the extended sources the flux density was obtained by means of TVSTAT.

The final list of radio sources (over the whole $\sim 1^\circ \times 1^\circ$ field), contains a total of 101 radio sources above the peak flux density limit of 0.20 mJy b^{-1} ; 52 radio sources out of the total are located in the $30' \times 30'$ region shown in Figure 2, and are presented in Table 3, where we give:

– columns 1, 2 and 3: respectively name (GMRT-) and J2000 position;

- column 4 and 5: respectively peak and integrated flux density at 610 MHz, corrected for the primary beam attenuation. Note that the flux density given for the relic source (J0454–1017a) does not include the embedded point sources, whose flux density was estimated from the full resolution image ($8.6'' \times 4.0''$, see Table 1) and subtracted;

- column 6: radio morphology. We classified the sources as unres.= unresolved and ext. = extended. Moreover we indicated as WAT a wide–angle–tailed morphology, D a double structure and Rel the relic source. For the double sources we give the position of the radio barycentre and for the extended sources we give the position of the radio peak.

We detected all the 20 radio sources found by A00 in their analysis of a portion of the 1.4 GHz NRAO VLA Sky Survey (NVSS, Condon et al. 1996) image, with a size similar to the field shown in Figure 2. We note that their sources labelled 12, 14 and 15 are part of the diffuse radio relic (see Section 6), and their sources labelled 7, 11 and 13 are part of the wide–angle tail described in Section 5.2. The remaining radio sources listed in Table 3 are either undetected or only marginally visible in the NVSS, due to the different resolution and the sensitivity limit of the NVSS survey ($1\sigma=0.45$ mJy b^{-1}).

5 Optical Identifications

The sample of 52 radio sources presented in the previous section was cross–correlated with the Super COSMOS/UKST Southern Sky Object Catalogue (Hambly et al. 2001) and the APM Catalogue (Maddox et al. 1990), to search for optical counterparts. Radio/optical overlays (using the DSS–1) were visually inspected for all the candidate identifications, and for the remaining radio sources in the sample, in order to find possible optical counterparts lost by the incompleteness of these catalogues.

We estimated the reliability of the optical identifications on the basis of the parameter R , which takes into account the uncertainty in the radio and optical positions:

$$R^2 = \frac{\Delta_{r-o}^2}{\sigma_o^2 + \sigma_r^2}$$

where Δ_{r-o} is the offset between the radio and optical coordinates, and σ_o and σ_r are the optical and the radio position errors respectively. We adopted a mean positional uncertainty of $\sigma_o=1.5$ arcsec for the optical catalogues (Unwin et al. 1993), and with the parameters of our observations we estimated

Table 3
Source list and flux density values

Name	RA _{J2000}	DEC _{J2000}	S _{peak}	S _{tot}	Radio Morphology
GMRT–			mJy b ⁻¹	mJy	
J0453–1023	04 53 02.69	–10 23 12.0	0.74	0.89	unres.
J0453–1020a	04 53 14.19	–10 20 05.4	0.54	0.67	unres.
J0453–1021	04 53 14.97	–10 21 33.0	0.68	0.91	unres.
J0453–1015	04 53 17.70	–10 15 58.0	0.53	0.59	unres.
J0453–1014	04 53 26.84	–10 14 19.7	74.43	96.56	unres.
J0453–1019a	04 53 44.72	–10 19 55.2	0.48	0.78	unres.
J0453–1011a	04 53 46.43	–10 11 09.3	0.72	0.79	unres.
J0453–1022	04 53 48.85	–10 22 43.5	0.45	0.64	unres.
J0453–0957	04 53 52.14	–09 57 59.0	4.84	49.73	D
J0453–1024	04 53 54.80	–10 24 08.2	3.72	4.59	unres.
J0453–1012	04 53 57.05	–10 12 41.7	0.51	0.54	unres.
J0453–1011b	04 53 57.23	–10 11 51.2	0.35	0.52	unres.
J0453–1018	04 53 58.04	–10 18 32.1	0.42	0.43	unres.
J0453–1019b	04 53 58.21	–10 19 21.4	0.89	0.90	unres.
J0453–1020b	04 53 59.87	–10 20 21.1	1.47	1.54	unres.
J0454–1002a	04 54 02.26	–10 02 07.0	3.68	9.11	ext.
J0454–1002b	04 54 03.45	–10 02 50.1	0.73	1.02	unres.
J0454–1013a	04 54 03.60	–10 13 00.1	0.33	0.33	unres.
J0454–1007	04 54 04.40	–10 07 53.5	16.43	36.77	D
J0454–1013b	04 54 06.90	–10 13 20.7	0.32	0.47	unres.
J0454–1012a	04 54 08.15	–10 12 55.0	0.31	0.46	unres.
J0454–1015	04 54 09.53	–10 15 09.6	1.47	1.49	unres.
J0454–1005a	04 54 10.79	–10 05 16.0	1.21	2.33	ext.
J0454–1004	04 54 10.82	–10 04 14.1	5.99	7.69	unres.
J0454–1013c	04 54 10.94	–10 13 43.6	0.27	0.33	unres.
J0454–1014a	04 54 11.66	–10 14 33.2	0.30	0.47	unres.
J0454–1002c	04 54 11.82	–10 02 59.00	5.37	7.46	unres.
J0454–1014b	04 54 12.08	–10 14 19.6	0.33	0.42	unres.
J0454–1011	04 54 13.71	–10 11 21.9	0.30	0.37	unres.

Table 3
Continued

J0454–1013d	04 54 13.93	–10 13 31.4	0.24	0.28	unres.
J0454–1009	04 54 15.39	–10 09 53.8	0.47	0.47	unres.
J0454–1005b	04 54 15.68	–10 05 42.8	1.84	2.89	unres.
J0454–1016a	04 54 16.28	–10 16 05.9	22.93	27.56	unres.
J0454–1006	04 54 16.33	–10 06 16.4	23.84	104.36	WAT
J0454–1019	04 54 19.34	–10 19 53.2	0.37	0.38	unres.
J0454–1017a	04 54 20	–10 17 00	–	41.9	Rel.
J0454–1016b	04 54 21.02	–10 16 44.2	1.77	3.85	unres.
J0454–1017b	04 54 22.34	–10 17 11.9	0.71	1.13	unres.
J0454–1008a	04 54 22.79	–10 08 26.9	0.38	0.38	unres.
J0454–1010	04 54 24.73	–10 10 09.4	1.01	1.04	unres.
J0454–1013c	04 54 29.60	–10 13 08.2	4.48	4.55	unres.
J0454–1005c	04 54 30.41	–10 05 09.8	1.14	1.27	unres.
J0454–1021a	04 54 35.33	–10 21 10.0	0.59	0.67	unres.
J0454–1008b	04 54 36.97	–10 08 30.0	0.39	0.40	unres.
J0454–1001	04 54 41.14	–10 01 37.6	16.54	24.35	unres.
J0454–1024	04 54 42.89	–10 24 17.5	0.70	0.93	ext.
J0454–1002d	04 54 44.20	–10 02 11.6	0.75	0.95	unres.
J0454–1020	04 54 46.79	–10 20 14.5	4.31	5.68	unres.
J0454–1014c	04 54 54.60	–10 14 06.5	5.42	6.82	unres.
J0454–1012b	04 54 55.54	–10 12 16.7	1.44	1.98	unres.
J0454–0955	04 54 57.27	–09 55 41.5	1.64	2.46	ext.
J0454–1013e	04 54 57.55	–10 13 33.0	3.82	5.24	unres.

an average radio positional error of 1 arcsec both in right ascension and declination (Prandoni et al. 2000).

We considered reliable identifications all matches with $R \leq 3$, i.e. we assume that all matches ≤ 3 are due to the random distribution of the positional errors, while for $R > 3$ the difference between the optical and radio position is significant. For two sources we found $R > 3$, and therefore we considered them uncertain identification (see notes to Table 4). We found 21 radio–optical identifications (including the 2 uncertain cases), which correspond to 40% of

our radio source sample.

In order to find the sources associated with A 521 member galaxies, we cross-correlated our sample of identified sources with the redshift catalogues in M00 and F03. We note that these two catalogues do not cover the full region of $30' \times 30'$ analysed in the present paper, therefore our redshift search is actually restricted to a region of $\sim 5'$ (1.1 Mpc) radius from the cluster centre (Fig. 2). This region includes 17 radio sources, 11 of which with an optical counterpart. Among these, 8 radio galaxies are located within the velocity range 70000 – 80000 km/s. One of them, however (J0454–1016b) is located in the group G2 (see Sect. 2), considered to be unbound in F03, therefore it will not be considered in the analysis presented in Sect. 5.3.

The list of the radio–optical identifications is reported in Table 4, where we give:

- column 1: radio and optical name, where FMC and MBP stands for optical counterparts from F03 and M00 respectively;
- columns 2 and 3: J2000 radio and optical coordinates;
- column 4: integrated flux density at 610 MHz and I magnitude given by the SuperCOSMOS or the APM catalogue when available, otherwise determined from the R magnitude adopting the $(R-I)=0.77$ colour for early–type galaxies at $z=0.2$ (Fukugita et al. 1995). The I magnitudes are corrected for a galactic absorption of $A_I=0.146$ (Schlegel et al. 1998); if they were derived from the R magnitudes, we first corrected these latter using an absorption $A_R=0.201$;
- column 5: radio morphology and $(R-I)$ colour from the SuperCOSMOS or the APM catalogue;
- column 6: radio power at 610 MHz and radial velocity;
- column 7: information about the galaxy type, and spectral features of the optical counterpart from M00 and F03 and R parameter. Note that for the extended radio galaxies discussed in Section 5.2, no value of R is given, due to the extended and complex radio morphology.

5.1 *Unresolved radio galaxies in the A 521 region*

Among the 8 cluster radio galaxies (see Table 4), we found three late–type and four early–type galaxies. One of them, J0454–1013b, is associated with the Brightest Cluster Galaxy (FMC65). For the remaining source, J0454–1016a, no colour information is available, however on the basis of its featureless spec-

Table 4
Optical Identifications

Radio Name	RA _{J2000}	DEC _{J2000}	$S_{610\text{MHz}}$	Radio type	$\log P_{610\text{MHz}}$	optical notes
GMRT–			(mJy)		(W Hz ⁻¹)	
Opt. Name	RA _{J2000}	DEC _{J2000}	I	(R-I)	v	R
					(km s ⁻¹)	
J0453–1023	04 53 02.69	–10 23 12.0	0.89	unres.	–	
	04 53 03.31	–10 23 06.2	16.20	0.93	–	6.0 (*)
J0453–1015	04 53 17.70	–10 15 58.0	0.59	unres.	–	
	04 53 17.62	–10 16 00.6	18.59	0.17	–	1.6
J0453–1019a	04 53 44.72	–10 19 55.2	0.77	unres.	–	
	04 53 44.45	–10 19 58.7	15.58	0.93	–	2.9
J0453–0957	04 53 52.14	–09 57 59.0	49.73	D	–	
	04 53 53.07	–09 58 35.4	16.76	1.00	–	–
J0453–1024	04 53 54.80	–10 24 08.2	4.59	unres.	–	
	04 53 55.25	–10 24 15.4	–	–	–	5.3 (**)
J0453–1012	04 53 57.05	–10 12 41.7	0.54	unres.	22.96	early-type
MBP20	04 53 57.00	–10 12 44.9	16.67	0.94	73044	1.8
J0453–1019b	04 53 58.21	–10 19 21.4	0.90	unres.	–	
	04 53 58.26	–10 19 21.0	18.67	–	–	0.4
J0454–1013a	04 54 03.60	–10 13 00.1	0.33	unres.	22.77	early-type
MBP14	04 54 03.58	–10 12 59.6	17.90	0.92	75146	0.3
J0454–1013b	04 54 06.90	–10 13 20.7	0.47	unres.	22.92	early-type, BCG
FMC65	04 54 06.84	–10 13 23.3	16.19	1.10	74372	1.5
J0454–1012a	04 54 08.15	–10 12 55.0	0.46	unres.	22.92	early-type
MBP11	04 54 08.11	–10 12 54.0	19.00	0.92	74873	0.6
J0454–1015	04 54 09.53	–10 15 09.6	1.49	unres.	22.85	
FMC90	04 54 09.33	–10 15 10.1	17.74	–	40747	1.7
J0454–1014a	04 54 11.66	–10 14 33.2	0.47	unres.	22.87	late-type, OII,OIIIa,b,H β
FMC105	04 54 11.72	–10 14 35.3	18.93	0.63	70952	1.2
J0454–1013d	04 54 13.93	–10 13 31.3	0.28	unres.	22.86	OII, Balmer
FMC121	04 54 13.90	–10 13 32.3	18.12	0.79	88714	0.6

Table 4
Continued

J0454–1016a	04 54 16.28	–10 16 05.9	27.56	unres.	24.69		
FMC143	04 54 16.34	–10 16 04.6	17.00	1.26	74282		0.9
J0454–1006	05 54 16.28	–10 06 16.4	103.36	WAT	–		
	05 54 16.05	–10 06 24.6	16.69	0.91	–		–
J0454–1016b	04 54 21.02	–10 16 44.2	3.85	unres.	23.88	late-type, OII, H β	
FMC170	04 54 20.96	–10 16 44.8	18.35	0.88	78326		0.5
J0454–1017b	04 54 22.34	–10 17 11.9	1.13	unres.	23.28	late-type, H β	
FMC178	04 54 22.35	–10 17 13.4	17.20	0.75	72593		0.8
J0454–1008a	04 54 22.79	–10 08 26.9	0.38	unres.	–		
	04 54 22.97	–10 08 25.7	18.05	–	–		1.6
J0454–1010	04 54 24.73	–10 10 09.4	1.04	unres.	–		
	04 54 24.65	–10 10 10.0	17.47	0.85	–		0.8
J0454–1005c	04 54 30.41	–10 05 09.8	1.27	unres.	–		
	04 54 30.25	–10 05 11.9	16.75	0.92	–		1.7
J0454–1008b	04 54 36.97	–10 08 30.0	0.39	unres.	–		
	04 54 36.72	–10 08 32.7	18.19	0.28	–		2.5

(*): this identification is uncertain since the candidate optical counterpart is misplaced with respect to the radio emission peak; (**): for the optical counterpart of this source only the magnitude $b_J=21.71$ is available. This galaxy falls within the radio contours of the source, but it is dislocated with respect to the emission peak.

trum (F03), and of the $(R-I)=1.26$ colour (taken from the SuperCOSMOS catalogue), we can *bona fide* classify it as an early-type galaxy.

For the cluster radio galaxies we searched for segregation effects both in the plane of the sky and in the velocity space.

In Figure 3 we show the distribution of the radio galaxies within 1.5 Mpc from the cluster centre, overlaid on the DSS–1 optical image and the X–ray isophotes from an archival ASCA observation (~ 45 ks). This X–ray image was extensively analysed in A00; the purpose of its use here is to illustrate the relative distribution of the hot gas and the positions of the cluster radio galaxies. The 8 radio galaxies of A 521 are represented by circles, while the two radio galaxies at a redshift different from A 521 are indicated by x–points. Squares show the location of radio sources identified with objects without redshift information, and diamonds are radio sources with no optical identification. Moreover the cross indicates the X–ray (ROSAT/HRI) centre

of the cluster (Tab. 1) and the blue large circles and ellipses represent the dynamical groups of optical galaxies found by F03 (Section 2, Fig. 1). The misplacement between the ROSAT cluster centre and the peaks of the ASCA isophotes can be explained as due to the lower resolution of the ASCA image, combined with the large uncertainties in the positional accuracy (A00).

It is clear that the radio galaxy distribution in A 521 is not random. In particular, all the radio galaxies within the cluster X-ray emission are aligned along the NW–SE axis, which is the suggested direction of the ongoing merger (A00, F05). On the other hand, no radio galaxy was detected along the old merger axis (roughly perpendicular to the NW–SE axis), where F03 found a ridge of high optical density. We note that a similar situation (at least in projection onto the plane of the sky) is found in A 2255 (Miller & Owen 2003), where the radio galaxies are distributed along the merger axis.

In Figure 4 the velocity distribution of the radio galaxies in A 521 is compared to the distribution of the whole velocity sample in M00 and F03 with secure velocity measurement. Objects corresponding to late-type radio galaxies are marked as black bins, the early-type radio galaxies are indicated by the dashed bin. The early-type objects are all found in the bins containing the bulk of the cluster galaxies, while the late-type radio galaxies are at the edge of the velocity distribution, even excluding the G2 member from these qualitative considerations. In particular, the three radio galaxies in the northern part of the G111 group (the BCG group, associated with the group detected in the X-ray) and the source belonging to G112 (see Figure 3) are all early-type galaxies, and are within a narrow range in velocity, i.e. $74282 \div 75146 \text{ km s}^{-1}$. F03 already noted that G111 and G112 are essentially at the same velocity within $\sim 200 \text{ km s}^{-1}$ (Sect. 2).

The remaining early-type radio galaxy of A 521 is the westernmost optical identification in Figure 3 and has a lower velocity (73044 km s^{-1}), consistent in redshift with the main cluster G11 (Fig. 1).

Among the late-type radio galaxies, one is located within the G111 group boundary (see Figure 3), but has a significantly lower velocity with respect to the group. The remaining two sources are embedded in the relic emission (Section 6) and projected within the G2 group. Of these two, J0454–1016b (the northwestern one) has a velocity consistent with the group, which is probably unbound to A 521, while the velocity of the other is significantly lower and consistent with the main cluster.

All the radio galaxies in A 521 have low radio power, exception made for J0454–1016a, located in projection close to the radio relic (see Table 4 and Figure 5), with $\log P_{610\text{MHz}} (\text{W Hz}^{-1}) = 24.69$. Interestingly, two late-type radio galaxies are more powerful than the early-type ones, suggesting enhanced star formation. Unfortunately, the data available in the literature do not allow

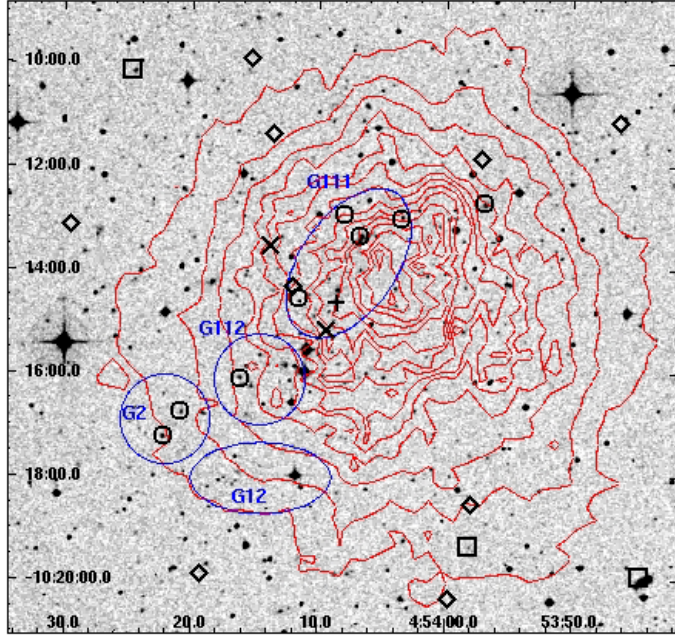


Fig. 3. Location of the radio sources within 1.5 Mpc from the A 521 centre, overlaid on the DSS-1 optical frame image and the X-ray ASCA contours. The cross indicates the ROSAT/HRI centre of the cluster (Tab.1). Circles represent the 8 radio galaxies belonging to A 521; the x-points represent the position of two radio galaxy located at a redshift different from A 521; squares are radio sources identified with an optical object without redshift information; diamonds are radio sources with no identified optical counterpart. Large blue circles and ellipses indicate the dynamical groups of optical galaxies. The X-ray contours are $3.0 \times 10^{-5} \div 2.4 \times 10^{-4}$ cts sec^{-1} and are spaced of 1.5×10^{-5} cts sec^{-1} .

to confirm this possibility.

5.2 Extended radio galaxies in the A 521 region

The radio galaxy population in A 521 is dominated by point-like low power objects. However, two extended radio galaxies are well visible in the northern region of the $30' \times 30'$ field of Figure 2. Their radio emission is overlaid on the DSS-1 in Figs. 6 (J0454-1006) and 7 (J0453-0957).

Unfortunately, no redshift information is available for the two optical counterparts, whose apparent magnitude is similar to that of the brightest cluster galaxies. Their (B-I) colour, derived from the SuperCOSMOS catalogue, is in very good agreement with the red sequence of the elliptical galaxies of the cluster, i.e. $\langle B - I \rangle \sim 2.6$ (see Fig.15 in F03). In particular, for J0454-1006 (B-I)=2.47 and for J0453-0957 (B-I)=2.64, therefore they might be part of A 521, despite the large distance from the cluster centre. If we assume that they are located at the average cluster distance, their total radio power is $\log P_{610\text{MHz}} = 25.26 \pm 0.08$ and $\log P_{610\text{MHz}} = 24.95 \pm 0.08$ for the wide-angle-tail

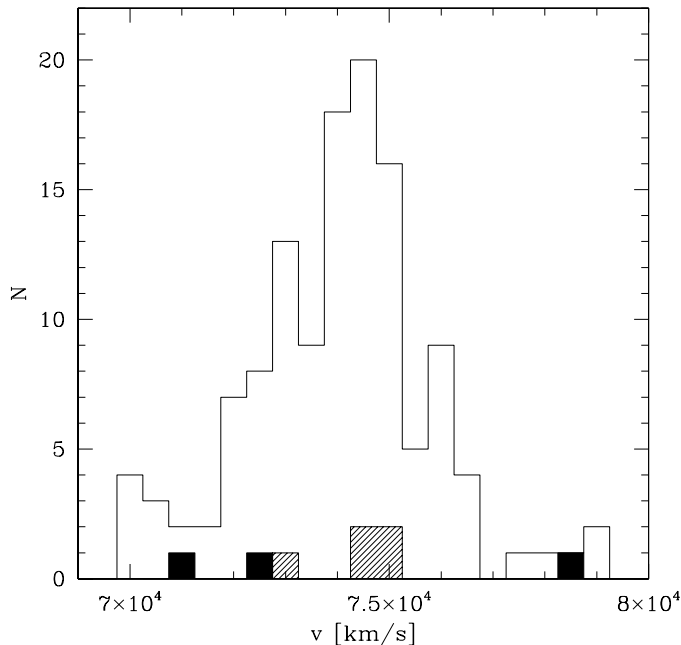


Fig. 4. Velocity distribution of the 8 radio galaxies of A 521 compared to the redshift distribution of cluster galaxies. Black bins represent late-type galaxies, dashed bins indicate early-type galaxies. The five galaxies with the highest velocity belong to the unbound group G2.

J0454–1006 and the source J0453–0957 respectively. These values are consistent with their radio structure, typical of intermediate power radio galaxies. The tailed morphology of J0454–1006 is suggestive of interaction between the radio plasma and the external medium. Furthermore, even though this source is outside the boundary of the cluster X-ray emission (Figs. 3 and 8), it is projected at a distance within the virial radius of A 521 (Tab. 1, Fig 2). Therefore its distorted radio structure may be the result of a recent accretion at the cluster virial radius. On the contrary, the morphology of J0453–0957, which is outside the virial radius, appears undisturbed.

5.3 AGN activity in A 521

In order to understand if the ongoing merger event in A 521 has significant effect on the radio emission of the AGN cluster population, it is useful to compare the number of observed radio galaxies in this merging environment with the number expected from the the radio luminosity function (RLF) for early-type galaxies in normal clusters and in the field. As reference we used the RLF at 1.4 GHz computed by Ledlow & Owen 1996, hereinafter LO96) for early-type galaxies in a sample of local Abell clusters. We are aware that the reference luminosity function was computed with a sample of clusters at lower

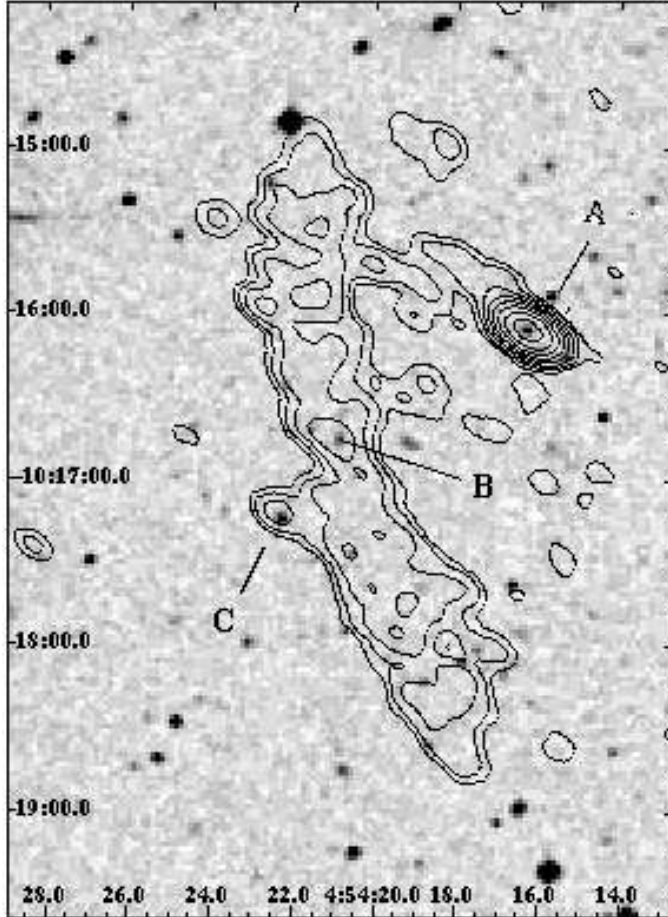


Fig. 5. 610 MHz contours of the diffuse radio source in A 521, overlaid on the DSS-1 optical frame. The radio contours are $0.12 \times (-1, 1, 2, 4, 8, 16, 32, 64, 128, 256, 512)$ mJy b^{-1} . The resolution is $13.1'' \times 8.1''$, in p.a. 56° . A, B and C indicates the position of radio galaxies embedded in the relic emission, i.e. the sources J0454-1016a, J0454-1016b and J0454-1017 respectively.

redshift, i.e. $z \leq 0.09$. Unfortunately, no statistical information on the RLF of cluster radio galaxies at the redshift of A 521 is available at present. This point will be further addressed in Section 7.

The analysis carried out by LO96 includes all radio galaxies within $0.3 R_A$ radius (R_A), with $\log P_{1.4\text{GHz}} (\text{W Hz}^{-1}) \geq 22.03$ and optical counterpart brighter than $M_R = -20.5$. This magnitude limit corresponds to $m_R = 19.8$ at the distance of the cluster A 521, and to the limit $I_{\text{lim}} = 19.0$, adopting the $(R-I) = 0.77$ colour for early-type galaxies at redshift $z = 0.2$, reported in Fukugita et al. 1995).

For full consistency with LO96 we restricted our analysis to the inner $0.3 R_A$, which corresponds to 2.9 arcmin at the redshift of A 521. The detection limit of our observations, i.e. 0.20 mJy, corresponds to $\log P_{1.4\text{GHz}} (\text{W Hz}^{-1}) = 22.14$ in the cosmology of LO96 and assuming a spectral index $\alpha = 0.8$

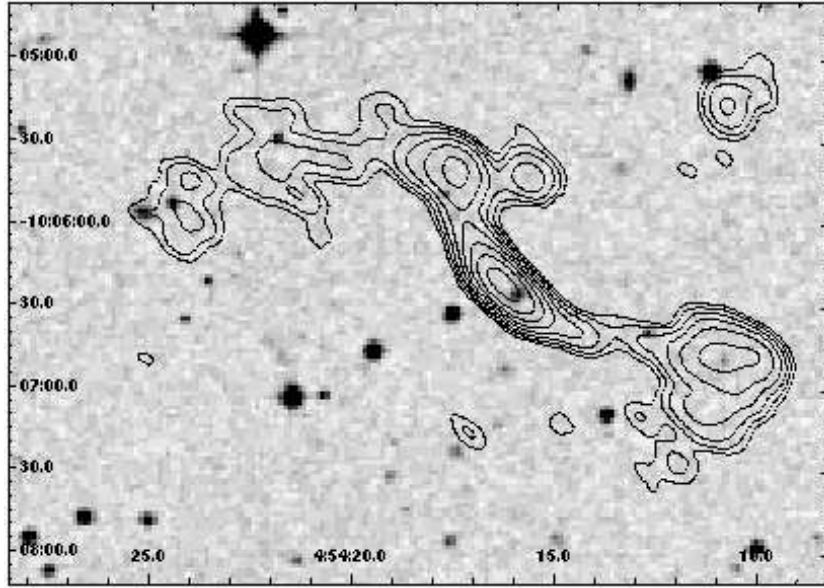


Fig. 6. 610 MHz contours of the wide-angle-tail radio source J0454–1006, located at the North of A 521, overlaid on the DSS–1 optical image. The radio contours are $0.12 \times (-1, 1, 2, 4, 8, 16, 32, 64, 128, 256, 512)$ mJy b^{-1} . The resolution is $13.1'' \times 8.1''$, in p.a. 56° . J0454–1005b is a point-like source, which is given as a separate source in Table 4.

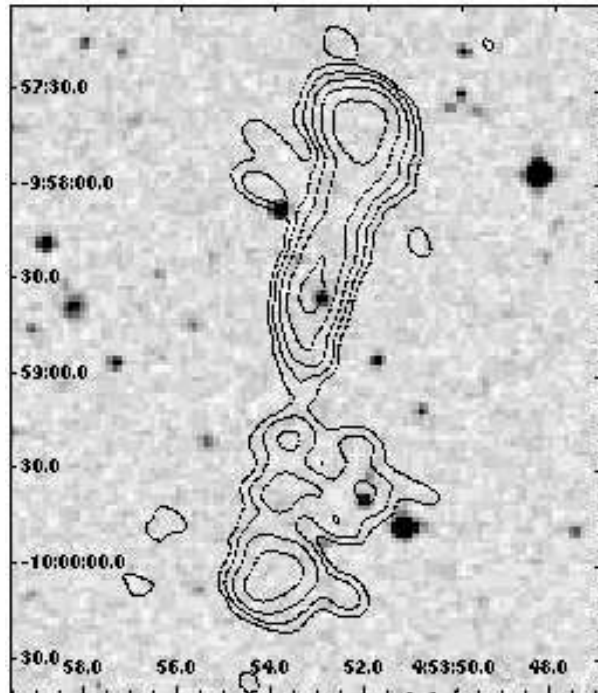


Fig. 7. 610 MHz contours of the extended radio source J0453–0957, located at the North of A 521, overlaid on the DSS–1 optical image. The radio contours are $0.12 \times (-1, 1, 2, 4, 8, 16, 32, 64, 128, 256, 512)$ mJy b^{-1} . The resolution is $13.1'' \times 8.1''$, in p.a. 56° .

(Condon 1992). In order to avoid our incompleteness in their first radio power bin, we compared the predictions from LO96 and our detections for $\log P_{1.4\text{GHz}} (\text{W Hz}^{-1}) \geq 22.43$, which corresponds to a flux limit $S_{610\text{MHz}} \simeq 0.36 \text{ mJy}$ (in our cosmology and again assuming $\alpha = 0.8$).

Three early-type radio galaxies of A 521 match the above constraints for the radio power and the optical magnitude, i.e. $\sim 4.7\%$ of the total.

The total number of early-type galaxies belonging to A 521 can be derived using the information in F03. A fraction of 57.6% of their spectroscopic sample is composed by early-type galaxies, and for $I < I_{lim}$, 85.5% of these objects are cluster members (see Figure 2 in F03). We corrected the number of early-type cluster galaxies for the incompleteness of the F03 spectroscopic sample, which is $\sim 55\%$ up to I_{lim} . We obtained that the total number of galaxies in the A 521 region brighter than I_{lim} is 131, of which 112 belonging to the cluster. Taking all these constraints into account, we end up with 64 early-type members in the inner $0.3 R_A$ of A 521.

On the basis of LO96, the expected number of radio emitting early-type galaxies is 6, i.e. $\sim 10\%$ of the total.

Allowing for the large poissonian uncertainties given by the small numbers we are dealing with, our 3 detections are consistent with the expectations from LO96 well within 1σ .

In Sect. 5.1 we pointed out the preferred location of the radio galaxies along the NW–SE axis. Unfortunately, the incomplete optical information (i.e. non-uniform coverage of A 521, see F03) does not allow any consideration on the connection between the distribution of the radio galaxies and that of the early-type objects in the cluster.

6 The relic source in A 521

The most remarkable feature of A 521 is the presence of a region of diffuse radio emission (Fig. 5) in the south-eastern peripheral part of the cluster, at a projected distance of ~ 4 arcmin (i.e. 930 kpc) from the A 521 centre, and at the border of the X-ray emission of the cluster (Figure 8).

The morphology of the source (labelled J0454–1017a in Table 3) is arc-shaped and highly elongated. Its total angular size along the major axis is $\sim 4'$, corresponding to a linear size of ~ 930 kpc, and its largest transversal angular size is only $\sim 50''$, corresponding to 200 kpc. This source was first detected at 1.4 GHz with the Very Large Array (VLA) by Ferrari (2003), and an image is

Table 5
Properties of the relic source in A 521.

$S_{610\text{MHz}}$ (mJy)	41.9 ± 2.1
$S_{1400\text{MHz}}$ (mJy)	16.2 ± 1.5
α_{610}^{1400}	1.14 ± 0.16
Linear size (kpc \times kpc)	$\sim 930 \times 200$
axial ratio	~ 4.5
d (arcmin) ¹	~ 4
$P_{610\text{MHz}}$ (10^{24} W Hz ⁻¹)	8.13
$P_{1400\text{MHz}}$ (10^{24} W Hz ⁻¹)	3.09
B'_{eq} (μG) ²	1.3

¹ distance from the cluster centre

² see Section 6

given also in the appendix of F05.

The resolution of the radio image in Figs. 5 and 8 is high enough to rule out the possibility that this object is a blend of different radio sources. If we exclude the cluster radio galaxies embedded in the diffuse emission (the point sources A, B and C in Fig. 5 and Table 4), the extended radio source does not appear to be associated with any optical counterpart.

The size and the radio morphology, as well as the lack of an optical identification, suggest that the diffuse radio source located at the outskirts of A 521 can be included in the class of cluster relics.

Fig. 5 also shows that the cluster radio galaxy A (J0454–1016a, the most powerful source in A 521) is located only 1.5' away from the relic (in the plane of the sky), and a faint bridge of radio emission connects the two sources. Even though projection effects in A 521 should be taken into account, we note that this situation is similar to what is found in the Coma cluster, where a bridge of radio emission connects the tails of the radio galaxy NGC 4789 and the prototype relic source 1253+275 (Giovannini et al. 1991).

In order to properly determine the value of the total flux density of the relic at 610 MHz, we integrated over the whole region covered by its emission and subtracted the flux density of the embedded point-sources (see Section 4). The flux density is $S_{610\text{MHz}} = 41.9\pm 2.1$ mJy, which gives a radio power $\log P_{610\text{MHz}}$ (W Hz⁻¹) = 24.91.

Using the NVSS information, we estimated the total spectral index of the relic between 610 MHz and 1400 MHz. The NVSS flux density at 1400 MHz is $S_{1400\text{MHz}} = 16.2\pm 1.5$ mJy (after subtraction of the embedded point sources),

and therefore $\alpha_{610MHz}^{1400MHz} = 1.14 \pm 0.16$.

A zero-order estimate of the energy density of the relativistic plasma and magnetic field associated with the relic can be obtained under the assumption of minimum energy conditions (e.g. Pacholczyk 1970). Assuming a power law spectrum for the electrons with slope $\delta = 2\alpha + 1$ ($\alpha = 1.14$), and the classical minimum energy equations (normally computed in the frequency range between $\nu_1=10$ MHz and $\nu_2=100$ GHz), we obtained an equipartition magnetic field $B_{eq}=0.4 \mu\text{G}$. However, we note that for this value of B_{eq} , the electrons with Lorentz factor $\gamma \sim 2.5 \times 10^3$ emit at 10 MHz, and thus the contribution of electrons with $\gamma < 2.5 \times 10^3$ to the total energy density is not taken into account. A more accurate approach is given by adopting equipartition equations with a low energy cut-off γ_{min} in the electron energy distribution (not in the emitted synchrotron spectrum). Using the equations given in Brunetti et al. 1997), we derived the following value for the magnetic field:

$$B'_{eq} \simeq 1.3 \times \left(\frac{\gamma_{min}}{50}\right)^{\frac{1-2\alpha}{\alpha+3}}$$

with B'_{eq} expressed in μG . The parameters of the relic source are given in Table 5 (B'_{eq} given for $\gamma_{min} = 50$).

Both values of the equipartition magnetic field are in agreement with the estimates found in the literature for radio relic sources and cluster radio halos, i.e. in the range $0.1 - 1 \mu\text{G}$ (see the review by Govoni & Feretti 2004).

7 Discussion

The main results of our 610 MHz GMRT study of A 521 can be summarized as follows.

- i) We detected a relic source, whose projected location is just at the boundary of the X-ray emission from the intracluster gas (Section 6);
- ii) We compared the number of detected radio loud AGN with the expectations from the radio luminosity function by LO96 (inner $0.3 R_A$ and $\log P_{1.4 \text{ GHz}}(\text{W Hz}^{-1}) \geq 22.43$) and found 3 objects, to be compared to the 6 expected (Section 5.3).

Point (i) is by far the most relevant. In the following we will discuss these results in the light of the assessed ongoing merger in this galaxy cluster.

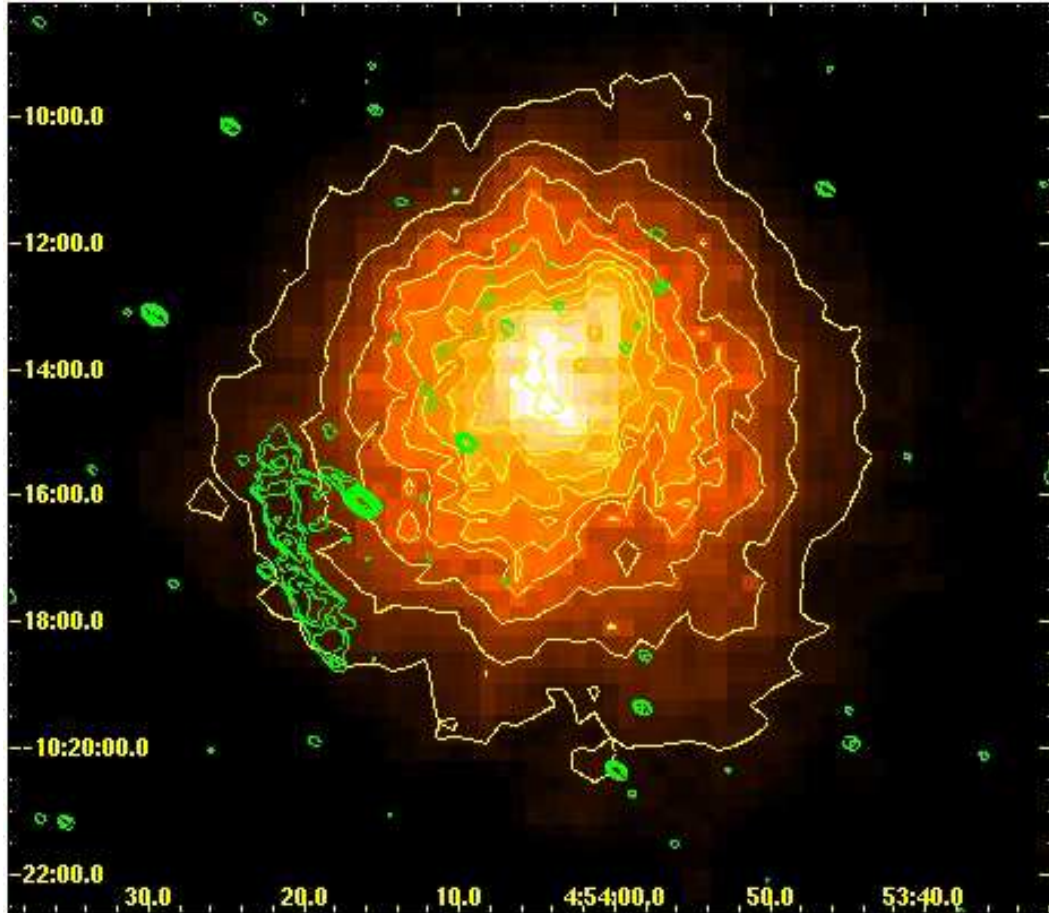


Fig. 8. 610 MHz radio contours (green) of the A 521 region, overlaid on the X-ray smoothed ASCA image (colours and yellow contours) of the cluster, extracted from the ASCA public archive. The resolution of the radio image is $13.1'' \times 8.1''$, in p.a. 56° . The first radio contour is the $5\sigma=0.2 \text{ mJy b}^{-1}$ level of the radio image. The X-ray contours are $3 \times 10^{-5} \div 2.4 \times 10^{-4} \text{ cts s}^{-1}$ and are spaced of $1.5 \times 10^{-5} \text{ cts s}^{-1}$.

7.1 Cluster merger and AGN/starburst radio activity

Our analysis on the cluster radio galaxies showed that the number of radio emitting early-type galaxies in the A 521 is consistent with the expectations from the standard RLF (3 against 6) if we allow for the large uncertainties due to the very small number statistics. Such comparison should be taken with care, since it is done with the local ($z \leq 0.09$) radio luminosity function for cluster ellipticals (see Section 5.3), while A 521 is at redshift 0.247. However, this result is striking if we take into account the positive evolution of the RLF for X-ray selected high redshift clusters (Stocke et al. 1999, Branchesi et al. 2005), and leads us to safely conclude that the multiple merger events in A 521 are not increasing the probability of an early-type galaxy to develop a nuclear radio source compared to other less extreme environments, as already

found in the complex merging environment of A 3558, in the central region of the Shapley Concentration (Venturi et al. 2000; Giacintucci et al. 2004).

The optical analysis of F03 showed that the late-type star forming galaxies, are preferentially located on the axis perpendicular to the direction of the merger (see Fig. 1). The radio power limit in our observations ($\log P_{610\text{MHz}} (\text{W Hz}^{-1}) = 22.54$) favours the detection of AGNs, so very little can be inferred on the role of the ongoing merger on the starburst activity in this cluster. However, if we consider $\log P_{610\text{MHz}} (\text{W Hz}^{-1}) = 23$ as a reasonable upper limit for the radio emission from starburst galaxies (e.g. Condon 1992), we can conclude that no major starburst emission is detected. Unfortunately, no information on the infrared flux of the late-type radio galaxies in our sample is available in the literature to give support to our conclusions.

7.2 *The merging events in A 521 and the formation of the relic*

The most important result of this paper is the detection of the relic source, which gives further observational support to the hypothesis of a close connection between cluster mergers and relic radio emission. The relic in A 521 is located in projection at the border of the cluster X-ray emission. It is slightly inclined with respect to the outer ring of the ASCA X-ray isophotes (see Fig. 8).

A number of models have been proposed to explain the origin of radio relics. All these models invoke a connection between these sources and the presence of a shock within the X-ray gas driven by a merging episode (see for instance Markevitch et al. 2005). Simulations of cluster mergers (Ricker & Sarazin, 2001) show that the merging of two subclusters leads to the formation of two shocks (front and back shock).

A 521 has a complex dynamics. The main cluster has a mass of the order of $10^{15} M_{\odot}$ and has been undergoing multiple minor merging events with groups whose mass is $\sim 1/10$ lower. Using the dynamical analysis of M00, F03 and F05, and from inspection of Figure 1, a possible scenario is that the group G111 is falling onto the main cluster G11, coming from North-West. Furthermore, the presence of the two optical groups G12 and G112 south of the central part of the cluster (see Figs. 1 and 3) suggests that also the southern part of the cluster region may be dynamically active.

7.2.1 *Merger shock*

One possibility is that relativistic electrons are accelerated from the thermal pool by the passage of a strong merger shock (Ensslin et al. 1998, Röttgering

et al. 1997). In this case the spectrum of the emitting electrons¹ is related to the Mach number M of the shock by

$$\delta = 2 \frac{(M^2 + 1)}{(M^2 - 1)} + 1$$

(e.g. Blandford & Eichler 1987). Here we include also the effect of particle aging $\Delta(\delta) = 1$, which comes out from the combined effect of Inverse Compton energy losses and continuous injection. In the case of A 521 the spectral index of the relic is $\alpha = 1.14$, which gives $\delta = 3.28$, and the requested Mach number of the shock is $M \sim 3.9$.

7.2.2 *Adiabatic compression*

A second possibility is adiabatic compression of fossil radio plasma by a merger shock (Ensslin & Gopal-Krishna 2001, hereinafter EG-K01). In this case, the numerical 3-D MHD simulations by Ensslin & Brüggen (2002, hereinafter EB02) predict a variety of radio morphologies and polarization properties, which may be reasonably well matched by the available high sensitivity radio images. Another important requirement in this scenario is the presence of an active radio galaxy in the proximity of the relic. This constraint is satisfied in A 521, where the radio galaxy J0454–1016a is located only 1.5' from the relic, i.e. a projected distance of ~ 350 kpc. A previous cycle of activity of this radio galaxy could have provided the fossil radio plasma in the ICM, revived by the shock compression.

7.2.3 *Ram pressure stripping*

Finally, another appealing possibility is that the relic in A 521 is the result of ram pressure stripping of the radio lobes of J0454–1016a (*a*) by group merger in the southern cluster region, or (*b*) by the infalling of J0454–1016a itself through G11.

This scenario requires that the internal pressure of the lobes P_{int} is significantly smaller than the external ram pressure, i.e.

$$P_{int} \approx 2 \frac{B_{eq}'^2}{8\pi} \ll \rho_{ICM} v_{merg}^2 \approx 10^{-12} n v_{merg}^2$$

where v_{merg} is the infalling velocity in units of 1000 km s^{-1} , ρ_{ICM} is the density of the intracluster medium, and n is the number density in units of 10^{-4}

¹ We do not consider the case of reacceleration of a pre-existing population of relativistic electrons (see Markevitch et al. 2005 for a detailed discussion).

particle cm^{-3} .

The projected distance of J0454–1016a from the relic (~ 350 kpc) requires a time of the order of

$$t_{cross} \approx 3.5 \times 10^8 \left(\frac{v_{merg}}{10^3 \text{km/s}} \right)^{-1} \text{ yr}$$

to be crossed by the ICM of any merging group (case *(a)*), or by J0454–1016a itself (case *(b)*). We note that in *(a)* we assume that the core position of J0454–1016a is not affected by the group merger dynamics. In order to allow the electrons in the radio lobes to still emit in the radio band, the time t_{cross} should be smaller than the life–time of the radiating electrons. This implies $v_{merg} \gtrsim 3000$ km/s. Such velocity leads to a Mach number $M \gtrsim 2$ for the merging group, or for J0454–1016a.

7.3 *Is there a shock in the external region of A 521?*

All the possibilities given above to explain the formation of a radio relic require the presence of a shock in the external region of A 521, with Mach number in the range $2 \lesssim M \lesssim 4$. In search for an observational signature of a shock in the relic region we re–analysed the public archive Chandra ACIS–I (39 ksec, OBSID 901) and ACIS–S (39 ksec OBSID 430) observations, analysed also in F05. We point out that the work in F05 is mainly restricted to the central and northern part of the cluster, and does not include the region which is relevant to the present discussion.

We processed the data using CIAO 3.2 and the newest calibration database CALDB 3.1.0. On the (0.5–5) keV background–subtracted and exposure–corrected image of the cluster, we extracted the radial X–ray surface brightness profile perpendicular to the relic source, using a 80° sector centered on the cluster centre and containing the relic.

The X–ray brightness profile does not show any evidence in support of the existence of a shock front at the projected location of the relic. This result is consistent with what we found in re–analysing the archive ASCA data (see also Fig. 8).

We point out, however, that this is not enough to rule out a connection between the relic and the presence of a shock. Two more issues should be considered. In particular: *(a)* the relic is very peripheral, therefore the cluster X–ray surface brightness is very low here, and deeper X–ray imaging is necessary to investigate the presence of a shock; *(b)* projection effects should also be taken into account in the analysis. We defer a detailed discussion on this point to a future paper.

8 Summary

In this paper we presented high sensitivity observations of the cluster of galaxies A 521, carried out at 610 MHz with the GMRT. The cluster is known to have a complex dynamics, and the radio emission from the cluster was analysed in detail, using the multiband (X-ray and optical) information available in the literature.

We found that the AGN activity in the cluster is consistent with the local RLF for cluster ellipticals within the large poissonian errors, i.e. we have 3 detections out of 6 expected sources. This result suggests that the multiple merging events in A 521 are not increasing the AGN radio activity in the early-type population compared to other environments.

A radio relic was detected at the cluster periphery, and a few possible scenarios for the presence of this relic were discussed.

One possibility is that the relic is connected to the presence of shock waves induced by the merger. Such shocks may have accelerated relativistic electrons or “revived” fossil radio plasma through adiabatic compression of the magnetic field or shock re-acceleration. The presence of an active cluster radio galaxy in the proximity of the relic suggests that the “revived” plasma might be connected to previous cycles of activity in this object. The radio properties of the relic require a high Mach number for such shock.

Another possible explanation is ram pressure stripping of radio lobes associated with the nearby radio galaxy J0454–1016a as a consequence of group infalling/merger. We showed that the projected distance between the relic and the radio galaxy may be in reasonable agreement with the age of the radiating electrons in such sources.

An analysis of public archive Chandra data does not provide observational evidence for the presence of a shock at the location of the relic, however projection effects should be taken into account for an accurate study.

We thank the staff of the GMRT for their help during the observations. GMRT is run by the National Centre for Radio Astrophysics of the Tata Institute of Fundamental Research. G.B. and R.C. acknowledge partial support from MIUR from grant PRIN2004. The authors wish to thank P. Mazzotta for insightful discussions and help with the analysis of the X-ray archive data.

References

Arnaud M., Maurogordato S., Slezak E., Rho J., 2000, *A&A*, 355, 461 (A00)

Bagchi J., Durret F., Neto G., Surajit P., Chavan S., 2005, 29th International Cosmic ray Conference, Pune, in press (astro-ph/0508013)

Blandford R. & Eichler D., 1987, Phys. Rep., 154, 1

Böhringer H., Schuecker P., Guzzo L., Collins C. A., Voges W., Cruddace R. G., Ortiz-Gil A., Chincarini G., De Grandi S., Edge, A. C., 2004, A&A, 425, 367

Branchesi M., Gioia I.M., Fanti C., Fanti R., Perley, R.A., 2005, A&A, in press (astro-ph/0509138)

Brunetti G., Setti G., Comastri A., 1997 A&A, 325, 898

Brunetti G., 2003, in *Matter and Energy in Clusters of Galaxies*, ASP Conf. Series 301, p.349

Brunetti G., in *Outskirts of galaxy clusters: intense life in the suburbs*, 2004, IAU colloquium 195, Ed. A. Diaferio, Cambridge Univ. Press, p.148

Buote D.A., 2001, ApJ, 553, L15

Cassano R., Brunetti G., Setti G., 2004, JKAS, 37, 589

Cassano R., Brunetti G., 2005, MNRAS, 357, 1313

Condon J.J., 1992, A&A Rev., 30, 575

Condon J.J., Cotton W.D., Greisen E.W, et al., 1996, ADIL, JC, 01

Ensslin T.A., Biermann P.L., Klein U., Kohle S., 1998, A&A 332, 395

Ensslin T.A., Brüggem M., 2002, MNRAS, 331, 1011 (EB02)

Ensslin T.A., Gopal-Krishna, 2001, A&A, 366, 26 (EG-K01)

Feretti L., Orrú E., Brunetti G., Giovannini G., Kassim N., Setti G., 2004, A&A, 423, 111

Feretti L., Fusco–Femiano R., Giovannini G., Govoni G., 2001, *A&A*, 373, 106

Feretti L., 2005, in *X-ray and Radio Connections*, eds. L.O. Sjouwerman & K.K Dyer, astro-ph/0406090

Ferrari C., 2003, Ph.D. Thesis, University of Nice–Sophia Antipolis, France

Ferrari C., Arnaud M., Ettore S., Maurogordato S., Rho J., 2005, *A&A*, in press (astro-ph/0508585) (F05)

Ferrari C., Maurogordato S., Cappi A., Benoist C., 2003, *A&A*, 399, 813 (F03)

Fukugita, M., Shimasaku, K., & Ichikawa, T., 1995, *PASP*, 107, 945

Giacintucci S., Venturi T., Bardelli S., Dallacasa D., Zucca E., 2004, *A&A*, 419, 71

Giacintucci S., Venturi T., Brunetti G., Bardelli S., Dallacasa D., Ettore S., Finoguenov A., Rao A.P., Zucca E., 2005, *A&A*, 440, 867

Giovannini G., Feretti L., Stanghellini C., 1991, *A&A*, 252, 528

Giovannini G., Feretti L., 2002, in *Merging Processes in Galaxy Clusters*, ed. L. Feretti, I.M. Gioia, G. Giovannini, *ASSL*, 272, 197

Giovannini G., Feretti L., 2004, *JKAS*, 37, 323

Govoni F., Feretti L., 2004, *Journal of Mod. Phys.*, Vol. 13, Issue 8, p. 1549

Hambly, N. C., MacGillivray, H. T., Read, M. A., Tritton, S. B., Thomson, E. B., Kelly, B. D., Morgan, D. H., Smith, R. E., Driver, S. P., Williamson, J., Parker, Q. A., Hawkins, M. R. S., Williams, P. M., Lawrence, A. 2001, *MNRAS*, 326, 1279

Kempner J.C., Sarazin C.L., 2001, *ApJ*, 548, 639

Ledlow M.J. & Owen F.N., 1996 *ApJ*, 112, 9 (LO96)

Maddox S.J., Efstathiou G., Sutherland W.J., Loveday J. 1990, *MNRAS*, 243, 692

- Markevitch M., Govoni F., Brunetti G., Jerius D., 2005, ApJ, 627, 733
- Maurogordato S., Proust D., Beers T.C., Arnaud M., Pelló R., Cappi A., Slezak E., Kriessler J.R., 2000, A&A, 355, 848, (M00)
- Miller N.A., Owen F.N., Hill J.M., 2003, AJ, 125, 2393
- Miller N.A., Owen F.N., 2003, AJ, 125, 2427
- Owen F.M., Ledlow M.J., Keel W.C., Morrison G.E., 1999, AJ, 118, 633
- Pacholczyk A.G., *Radio Astrophysics*, 1970, Freeman Eds.
- Prandoni I., Gregorini L., Parma P. et al. 2000, A&AS, 146, 41
- Reiprich T.H. & Böhringer H., 2002, ApJ, 567, 716
- Ricker P. M. & Sarazin C. L., 2001, ApJ, 561, 621
- Roettiger K., Burns J.O., Stone J.M., 1999, ApJ, 518, 603
- Röttgering H.J.A, Wieringa M.H., Hunstead R.W., Ekers R.D., 1997, MNRAS 290, 577
- Sarazin C.L., 2002, in *Merging Processes in Galaxy Clusters*, ed. L. Feretti, I.M. Gioia, G. Giovannini, ASSL, 272, 1
- Sarazin C.L., 2004, in *X-ray and radio connections meeting*, ed. L. O. Sjouwerman & K. K. Dyer, astro-ph/0406181
- Schlegel D.J., Finkbeiner D.P., Davis M., 1998, ApJ, 500, 525
- Schuecker P., Bhringer H., Reiprich T.H., Feretti L., 2001, A&A, 378, 408
- Stoche J.T., Perlman E.S., Gioia I.M., Harvanek M., 1999, AJ 117, 1967
- Unewisse A.M., Hunstead D.W. & Pietrzynski B., 1993, Publ. Astron. Soc. Austr., 10, 229

Venturi T., Bardelli S., Morganti R., Hunstead R.W., 2000, MNRAS, 314, 594

Venturi T., Bardelli S., Dallacasa D., Brunetti G., Giacintucci S., Hunstead R.W., Morganti R., 2003, A&A, 402, 913